Bi-orthogonal Wavelet System for High-Resolution Image Reconstruction

Lixin Shen[†] and Qiyu Sun

Abstract

High-resolution images are often desired but made impossible because of hardware limitation. For the high-resolution model proposed by Bose and Boo, the iterative wavelet-based algorithm has been shown to perform better than traditional least square method when the resolution ratio M is two and four. In this paper, we discuss the minimally supported bi-orthogonal wavelet system arisen from the mathematical model by Bose and Boo, and propose a wavelet-based algorithm for arbitrary resolution ratio $M \geq 2$. The numerical results indicate that the algorithm based on our bi-orthogonal wavelet system performs better in high-resolution image reconstruction than the wavelet-based algorithm in the literature and also the common-used least square method.

Index Terms

High-resolution image reconstruction, deblurring, multiresolution analysis, bi-orthogonal wavelets.

EDICS Category: 2-MWAV

[†]L. Shen (corresponding author) is with the Department of Mathematics, Armstrong Hall, P. O. Box 6310, West Virginia University, Morgantown, WV 26505. The telephone number is (304)293-2011. The fax number is (304)-293-3982. Email address: lshen@math.wvu.edu

Q. Sun is with the Department of Mathematics, University of Central Florida, Orlando, FL 32816-1364. The telephone number is (407)-823-4839. The fax number is (407)-823-6253. Email address: qsun@mail.ucf.edu

I. INTRODUCTION

High-resolution images are often desired in many situations, such as remote sensing and medical imaging, but made impossible because of hardware limitations. Then increasing the resolution by image processing techniques is of great importance. The earliest formulation of the problem of high-resolution image reconstruction was proposed by Huang and Tsay [1] in 1984, where it was motivated by the need of improved resolution images from Landsat image data. This work has drawn a lot of research attention and has been extensively treated in the last three decades [2], [3], [4], [5], [6], [7], [8], [9], [10], [11], [12], [13], [14], [15], [16], [17]. Applications of high-resolution image construction arise in many areas. The main idea is to recover a single high-resolution image from a set of low quality images of a true image.

The model in Bose and Boo [9] concentrates on reconstructing one high-resolution image from multiple low-resolution, shifted, degraded samples of a true image. That model was first analyzed from a wavelet point of view for both the case with no displacement error [18] and the case with displacement error [19]. In [18], we followed the approach in [9] and considered the case where the blur is spatially invariant, i.e., there are no displacement errors in the low-resolution samples. By expressing the true image (high-resolution image) as a function in $L^2(\mathbb{R}^2)$, we derived an iterative algorithm which recovers the function completely in the L^2 sense from the given low-resolution functions. These algorithms decompose the function obtained from the previous iteration into different frequency components in the wavelet transform domain, and then add them into the new iterate to improve the approximation. Wavelet thresholding methods [20] are applied to de-noise the function obtained in the previous step before adding it to the new iterate. In [19], we considered the case where there are displacement errors in the low-resolution samples. The resulting blurring operator is spatially varying and is formed by sampling and summing different spatially invariant blurring operators. We represented each of these spatially invariant blurring operators by a tensor product of a low pass filter which associates the corresponding blurring operator with a multiresolution analysis of $L^2(\mathbb{R}^2)$. That low pass filter is a tensor product of the univariate low pass filter

$$\frac{1}{M}\Big[\frac{1}{2} + \epsilon, \ \underbrace{1, \ \ldots, \ 1}_{M-1}, \ \frac{1}{2} - \epsilon\Big], \tag{1}$$

where M is the ratio between high and low resolutions. We will refer to the filter of (1) as (M, ϵ) high-resolution filter ((M, ϵ)-HRF). For $M = 2$ and $M = 4$, it was shown in [18] and [19] that the sequence (1) is a primal low pass filter in a bi-orthogonal wavelet system, and that the corresponding wavelet-based algorithms give better results than the existing method [9], [11] in terms of high output quality

and low relative errors. In this paper, we design the minimally supported bi-orthogonal wavelet system, whose prime low pass filter is the (M, ϵ)-HRF, for arbitrary resolution ratio $M \geq 2$ and displacement error $\epsilon \in (-\frac{1}{2}, \frac{1}{2})$, and we apply the corresponding wavelet-based algorithm to the high-resolution image reconstruction. The numerical results show that the wavelet-based algorithm with the minimally supported filters designed in this paper performs better than the least square methods (see for example [21]) in the image quality and peak signal-to-noise ratio (PSNR), and the similar wavelet-based algorithm with different filters ([19]) in less artifacts.

This paper is organized as follows. In Section II, we briefly recall the mathematical model for high-resolution image reconstruction and preliminary theory for the bi-orthogonal wavelets with dilation $M \geq 2$. In Section III, we first show that the (M, ϵ)-HRF is the low pass filter associated with a multiresolution analysis with dilation M. Next, we present a method to design the dual low pass filter of (M, ϵ)-HRF from the one of $(M, 0)$-HRF. Finally we prove the (M, ϵ)-HRF and its dual are the low pass filters associated with two bi-orthogonal multiresolution analyses with dilation M. In Section IV, a bi-orthogonal wavelet filter bank with (M, ϵ)-HRF as the low pass filter is constructed explicitly. The numerical experiments for the designed wavelet filter bank are presented in Section V. The conclusion of this paper is given in Section VI.

Notations: Bold-faced characters indicate vectors and matrices. The matrix $\mathbf{L}^T$ denotes the transpose of the matrix $\mathbf{L}$. Symbol $\mathbf{I}$ and $\mathbf{0}$ denote the identity and zero matrices respectively. Throughout the paper, j will denote $\sqrt{-1}$. For a given function $f \in L^1(\mathbb{R})$, $\widehat{f}(\omega) = \int_{\mathbb{R}} f(x) e^{-jx\omega} \, dx$ will denote the Fourier transform of f. For a given sequence m, $\widehat{m}(\omega) = \sum_{k \in \mathbb{Z}} m(k) e^{-jk\omega}$ will denote the Fourier series of m. $\widehat{m}^*$ denotes the complex conjugate of $\widehat{m}$. The Kronecker character $\delta_{k,l} = 1$ if $k = l$ and 0 otherwise. The ℓ^2 norm $\|u\|_2$ of a sequence $u := \{u(k)\}_{k \in \mathbb{Z}}$ is $\|u\|_2 = \left(\sum_{k \in \mathbb{Z}} |u(k)|^2 \right)^{1/2}$. The difference operator ∇ is defined by $\nabla v(k) = v(k) - v(k+1)$, $k \in \mathbb{Z}$, where $v := \{v(k)\}_{k \in \mathbb{Z}}$.

II. MATHEMATICAL MODEL AND BI-ORTHOGONAL WAVELETS

This section includes two parts. In the first part, we briefly describe the mathematical model of the high-resolution image reconstruction problem, and introduce a wavelet-based high-resolution image reconstruction algorithm for any given ratio $M \geq 2$ and any horizontal and vertical displacement errors ϵ^x, ϵ^y in $(-\frac{1}{2}, \frac{1}{2})$. Preliminaries of the bi-orthogonal wavelet theory is given in the second part.

A. Mathematical Model

Let the intensity function of an underlying continuous image be $f(x, y)$. The model assumes that an image at a given resolution is obtained by means of averaging f over the pixels which have size corresponding to that resolution. The mathematical problem is: given several averages of f at a low resolution, how can we deduce a good approximation to an average of f at a higher resolution?

Suppose that the image of a given scene can be obtained from sensors with $N_1 \times N_2$ pixels. Let the actual length and width of each pixel be T_1 and T_2 respectively. Our aim is to construct a higher resolution image by using an array of $M_1 \times M_2$ low-resolution sensors, i.e., we want an image with $K_1 \times K_2$ pixels, where $K_1 = M_1 N_1$ and $K_2 = M_2 N_2$. Thus the length and width of each of these high-resolution pixels will be T_1/M_1 and T_2/M_2 respectively. To maintain the aspect ratio of the reconstructed image, we consider only $M_1 = M_2 = M$. By reconstructing the high-resolution image, we mean to find or approximate the values which is the average intensity of all the points inside the (p, q)th high-resolution pixel. In order to have enough information to resolve the high-resolution image, there are subpixel displacements between the sensors in the sensor arrays. For sensor (m_1, m_2), $0 \le m_1, m_2 < M$ with $(m_1, m_2) \ne (0, 0)$, its horizontal and vertical displacements $d^x_{m_1, m_2}$ and $d^y_{m_1, m_2}$ with respect to the $(0, 0)$ reference sensor are given by $d^x_{m_1, m_2} = \left(m_1 + \epsilon^x_{m_1, m_2}\right) \frac{T_1}{M}$ and $d^y_{m_1, m_2} = (m_2 + \epsilon^y_{m_1, m_2}) \frac{T_2}{M}$. Here $\epsilon^x_{m_1, m_2}$ and $\epsilon^y_{m_1, m_2}$ are the horizontal and vertical displacement errors respectively. For sensor (m_1, m_2), the values $g_{m_1, m_2}[n_1, n_2]$ registered at its (n_1, n_2)th pixel is modeled by the average intensity of all points inside the low-resolution pixels and contaminated then by noise. The $K_1 \times K_2$ observed high-resolution image g is formed from all the low-resolution images g_{m_1, m_2} by assigning $g[Mn_1 + m_1, Mn_2 + m_2] = g_{m_1, m_2}[n_1, n_2]$.

The blurring matrix for the whole sensor array is made up of matrices from each sensor:

$$\mathbf{L}(\boldsymbol{\epsilon}^x, \boldsymbol{\epsilon}^y) = \sum_{m_1=0}^{M-1} \sum_{m_2=0}^{M-1} \mathbf{D}_{m_1, m_2} \mathbf{L}(\epsilon^x_{m_1, m_2}, \epsilon^y_{m_1, m_2}).$$

Here both $\boldsymbol{\epsilon}^x$ and $\boldsymbol{\epsilon}^y$ are $M \times M$ matrices; $\mathbf{D}_{m_1, m_2}$ are $K_1 K_2 \times K_1 K_2$ sampling matrices, which are diagonal matrices with diagonal elements equal to 1 if the corresponding component of g comes from the (m_1, m_2)th sensor and zero otherwise; $\mathbf{L}(\epsilon^x_{m_1, m_2}, \epsilon^y_{m_1, m_2})$ is the Kronecker product of $\mathbf{L}(\epsilon^x_{m_1, m_2})$ and $\mathbf{L}(\epsilon^y_{m_1, m_2})$, i.e., $\mathbf{L}(\epsilon^x_{m_1, m_2}, \epsilon^y_{m_1, m_2}) = \mathbf{L}(\epsilon^x_{m_1, m_2}) \otimes \mathbf{L}(\epsilon^y_{m_1, m_2})$, where $\mathbf{L}(\epsilon^x_{m_1, m_2})$ is an $K_2 \times K_2$ circular matrix (under periodic boundary condition) with the middle row given by

$$\frac{1}{M} \Big[0, \cdots, 0, \frac{1}{2} + \epsilon^x_{m_1, m_2}, \underbrace{1, \ldots, 1}_{M-1}, \frac{1}{2} - \epsilon^x_{m_1, m_2}, 0, \cdots, 0\Big] \tag{2}$$

(there are $K_2 - M - 1$ zero components) and similarly for the $K_1 \times K_1$ blurring matrix $\mathbf{L}(\epsilon^y_{m_1, m_2})$. The

reconstruction of high-resolution image can be modeled as solving

$$\mathbf{L}(\epsilon^x, \epsilon^y)\mathbf{f} = \mathbf{g}, \tag{3}$$

where $\mathbf{f}$ and $\mathbf{g}$ are the column vectors formed by f and g respectively. The blurring matrix $\mathbf{L}(\epsilon^x_{m_1,m_2}, \epsilon^y_{m_1,m_2})$ corresponding to the (m_1, m_2)th sensor can be considered as a low pass filter acting on the image f. This low pass filter is a tensor product of the (M, ϵ)-HRF (see (1) and (2)), where the parameters ϵ are different in the x and y directions for each sensor.

To introduce the wavelet-based high-resolution image reconstruction algorithm, we only consider the case $\epsilon^x_{m_1,m_2} = \epsilon^x$ and $\epsilon^y_{m_1,m_2} = \epsilon^y$ for all $0 \le m_1, m_2 < M$. Moreover, the displacement error satisfies the physical requirement $|\epsilon^x|, |\epsilon^y| < 1/2$ (see, e.g. [9] and [19]). In that case, the blurring matrix $\mathbf{L} = \mathbf{L}(\epsilon^x, \epsilon^y)$ in (3) becomes $\mathbf{L}(\epsilon^x) \otimes \mathbf{L}(\epsilon^y)$, where $\mathbf{L}(\epsilon)$ is the matrix representation of the (M, ϵ)-HRF. Starting from the low pass filter (M, ϵ)-HRF, we construct dual low pass filters $_{M,\epsilon}\widetilde{m}_0$, high pass filter bank $_{M,\epsilon}m_t, 1 \le t \le M - 1$, and dual high pass filter bank $_{M,\epsilon}\widetilde{m}_t, 1 \le t \le M - 1$, for any $\epsilon \in (-\frac{1}{2}, \frac{1}{2})$ in the following two sections. This leads to a perfect reconstruction of that bi-orthogonal wavelet system

$$\widetilde{\mathbf{L}}^T(\epsilon)\mathbf{L}(\epsilon) + \sum_{t=1}^{M-1} \widetilde{\mathbf{G}}_t^T(\epsilon)\mathbf{G}_t(\epsilon) = \mathbf{I},$$

where $\widetilde{\mathbf{L}}(\epsilon), \mathbf{G}_t(\epsilon), \widetilde{\mathbf{G}}_t(\epsilon), 1 \le t \le M - 1$, are the matrix representation of the corresponding dual low pass filter, high pass filter bank, and dual high pass filter bank, respectively. Define $\widetilde{\mathbf{L}} = \widetilde{\mathbf{L}}(\epsilon^x) \otimes \widetilde{\mathbf{L}}(\epsilon^y)$, $\mathbf{G}_{0t'} = \mathbf{L}(\epsilon^x) \otimes \mathbf{G}_{t'}(\epsilon^y)$, $\mathbf{G}_{t0} = \mathbf{G}_t(\epsilon^x) \otimes \mathbf{L}(\epsilon^y)$, and $\mathbf{G}_{tt'} = \mathbf{G}_t(\epsilon^x) \otimes \mathbf{G}_{t'}(\epsilon^y)$, where $1 \le t, t' \le M - 1$. Similarly we define $\widetilde{\mathbf{G}}_{tt'}$ for all $0 \le t, t' \le M - 1$ except $(t, t') = (0, 0)$. These matrices satisfy

$$\widetilde{\mathbf{L}}^T\mathbf{L} + \sum_{\substack{0 \le t,t' \le M-1 \\ (t,t') \ne (0,0)}} \widetilde{\mathbf{G}}_{tt'}^T \mathbf{G}_{tt'} = \mathbf{I}$$

(see [22], [23], [24], [25], [26]). Then the following iterative wavelet-based high-resolution image reconstruction algorithm is used to approximate the solution of the equation (3):

$$\mathbf{f}_{n+1} = \widetilde{\mathbf{L}}^T\mathbf{g} + \sum_{\substack{0 \le t,t' \le M-1 \\ (t,t') \ne (0,0)}} \widetilde{\mathbf{G}}_{tt'}^T \mathcal{T}(\mathbf{G}_{tt'}\mathbf{f}_n) \tag{4}$$

for $n \ge 0$ with the initial $\mathbf{f}_0 = 0$, where $\mathcal{T}$ is the thresholding operator [20]. When the resolution ratio M of the reconstruction image is 2 or 4, the above iterative reconstruction algorithm reduces to the algorithm in [18] and [19]. However, we should point it out that matrices $\widetilde{\mathbf{L}}, \mathbf{G}_{tt'}$, and $\widetilde{\mathbf{G}}_{tt'}$ are different from those in [18] and [19].

B. Bi-orthogonal Wavelet System with Dilation M

In this section, we recall some basic theory for bi-orthogonal wavelets necessary for our later exposition. For a more complete and rigorous presentation, interested readers may refer to [24], [25], [26] and [27].

We start from a compactly supported scaling function ϕ and the corresponding multiresolution analysis with dilation M. An multiresolution analysis with dilation M is a family of closed subspaces $\{V_n\}_{n\in\mathbb{Z}}$ of $L^2(\mathbb{R})$ that satisfies 1) $\bigcup_n V_n$ is dense in $L^2(\mathbb{R})$ and $\bigcap_n V_n = \{0\}$; 2) $V_n \subset V_{n+1}$ and $f(\cdot) \in V_n$ if and only if $f(M\cdot) \in V_{n+1}$ for all n; 3) $\{\phi(x - k) : k \in \mathbb{Z}\}$ forms a Riesz basis of the shift invariant space V_0.

The scaling function ϕ satisfies a refinement equation

$$\phi(x) = M \sum_{k\in\mathbb{Z}} m_0(k)\phi(Mx - k) \tag{5}$$

and the normalization condition $\widehat{\phi}(0) = 1$, where the finitely supported sequence m_0 on $\mathbb{Z}$ satisfies $\sum_{k\in\mathbb{Z}} m_0(k) = 1$. If $\phi \in L^2(\mathbb{R})$ and its shifts form a Riesz basis of the corresponding shift invariant space, then we call ϕ stable. It is known ([24], [25], [26]) that ϕ is a scaling function of some multiresolution if and only if ϕ is a stable function in L^2 and satisfies a refinement equation of the form (5).

Taking the Fourier transform on both sides of (5), we have

$$\widehat{\phi}(\omega) = \widehat{m}_0\left(\frac{\omega}{M}\right)\widehat{\phi}\left(\frac{\omega}{M}\right), \quad \omega \in \mathbb{R}. \tag{6}$$

We call $\widehat{m}_0$ the symbol of the scaling function ϕ. Very often, we also call m_0 or $\widehat{m}_0$ the low pass filter. Applying (6) iteratively for n times yields

$$\widehat{\phi}(\omega) = \prod_{i=1}^{n} \widehat{m}_0\left(\frac{\omega}{M^i}\right)\widehat{\phi}\left(\frac{\omega}{M^n}\right).$$

Letting n tend to infinity in the above equation and using the normalization condition of ϕ, we then obtain the explicit expression of $\widehat{\phi}$ via its corresponding low pass filter $\widehat{m}_0$,

$$\widehat{\phi}(\omega) = \prod_{i=1}^{\infty} \widehat{m}_0\left(\frac{\omega}{M^i}\right).$$

A function $\widetilde{\phi} \in L^2(\mathbb{R})$ is called a dual function of $\phi \in L^2(\mathbb{R})$ if

$$\int_{\mathbb{R}} \phi(x - k)\widetilde{\phi}(x - k')dx = \delta_{k,k'} \quad \forall\, k, k' \in \mathbb{Z}. \tag{7}$$

Often we call ϕ and $\widetilde{\phi}$ a dual pair. In the bi-orthogonal wavelet setting, there are two multiresolution analyses, $\{V_n\}$ and $\{\widetilde{V}_n\}$, whose scaling functions ϕ and $\widetilde{\phi}$ form a dual pair. For a dual pair of scaling

functions ϕ and $\widetilde{\phi}$, it follows from (5) and (7) that their corresponding low pass filters $\widehat{m}_0$ and $\widehat{\widetilde{m}}_0$ satisfy

$$\sum_{t=0}^{M-1} \widehat{m}_0(\xi + \vartheta_t)\widehat{\widetilde{m}}_0^*(\xi + \vartheta_t) = 1,$$

where $\vartheta_t = \frac{2\pi t}{M}$, $t = 0, 1, \cdots, M - 1$. By matrix extension ([28], [29]), there exist $\widehat{m}_s$ and $\widehat{\widetilde{m}}_s, s = 1, \ldots, M - 1$, so that

$$\sum_{t=0}^{M-1} \widehat{m}_s(\omega + \vartheta_t)\widehat{\widetilde{m}}_{s'}^*(\omega + \vartheta_t) = \delta_{s,s'} \tag{8}$$

for all $s, s' = 0, \ldots, M - 1$. This implies the perfect reconstruction for the analysis filter banks $\widehat{m}_s, 0 \leq s \leq M - 1$, and the synthesis filter bank $\widehat{\widetilde{m}}_s, 0 \leq s \leq M - 1$:

$$\sum_{s=0}^{M-1} \widehat{m}_s(\omega)\widehat{\widetilde{m}}_s^*(\omega + \vartheta_t) = \delta_{t,0},$$

where $t = 0, \ldots, M - 1$. We mention that filters m_0 and $\widetilde{m}_0$ to be low pass, and that m_s and $\widetilde{m}_s$, $s = 1, \cdots, M - 1$, to be high pass, in the sense that

$$\widehat{m}_0(\vartheta_k) = \widehat{\widetilde{m}}_0(\vartheta_k) = \delta_{k,0},$$

$$\widehat{m}_s(0) = \widehat{\widetilde{m}}_s(0) = 0, \quad s = 1, \cdots, M - 1.$$

By (7) and (8), the functions ψ_s and $\widetilde{\psi}_s, 1 \leq s \leq M - 1$, which are defined by

$$\widehat{\psi}_s(\omega) = \widehat{m}_s\left(\frac{\omega}{M}\right)\widehat{\phi}\left(\frac{\omega}{M}\right), \quad \widehat{\widetilde{\psi}}_s(\omega) = \widehat{\widetilde{m}}_s\left(\frac{\omega}{M}\right)\widehat{\widetilde{\phi}}\left(\frac{\omega}{M}\right),$$

are multi-band bi-orthogonal wavelets constructed from the multiresolution analyses $\{V_n\}$ and $\{\widetilde{V}_n\}$. Therefore starting from a dual pair of scaling functions ϕ and $\widetilde{\phi}$, the construction of bi-orthogonal wavelets ψ_s and $\widetilde{\psi}_s, 1 \leq s \leq M - 1$, reduces to the construction of high pass filters $\widehat{m}_s$ and $\widehat{\widetilde{m}}_s, 1 \leq s \leq M - 1$, so that they together with the low pass filters $\widehat{m}_0$ and $\widehat{\widetilde{m}}_0$ of the scaling functions ϕ and $\widetilde{\phi}$ satisfy the perfect reconstruction condition (8).

III. The High-Resolution Filter and Its Dual

In this section, we show that i) the (M, ϵ)-HRF is the low pass filter of a scaling function; ii) the dual filters with displacement error can be deviated from the ones with no displacement error; and iii) the minimally supported dual filter is the low pass filter of a dual scaling function.

The index of the high-resolution filter (M, ϵ)-HRF, which is formulated in the mathematical model for the reconstruction of a high-resolution image, starts from $-\lfloor \frac{M}{2} \rfloor$ to $\lfloor \frac{M+1}{2} \rfloor$. Here $\lfloor y \rfloor$ denotes the largest integer not exceeding y. Note that if $\widehat{m}_s(\omega), \widehat{\widetilde{m}}_s(\omega), 0 \leq s \leq M - 1$, satisfy (8), then so do $e^{jk_0\omega}\widehat{m}_s(\omega)$, $e^{jk_0\omega}\widehat{\widetilde{m}}_s(\omega), 0 \leq s \leq M - 1$, where $k_0 \in \mathbb{Z}$. Thus we assume that the index of the high-resolution filter

(M, ϵ)-HRF starts from 0 to M instead. We denote that filter by $_{M,\epsilon}m_0$, and denote $_{M,0}m_0$ as $_{M}m_0$ when there is no displacement error. Also notice that $_{M,-\epsilon}\widehat{m}_0(\omega) = e^{-jM\omega} {}_{M,\epsilon}\widehat{m}_0(-\omega)$, and that if $\widehat{m}_s(\omega), \widehat{\widetilde{m}}_s(\omega), 0 \leq s \leq M-1$, satisfy (8) then so do $\widehat{m}_s(-\omega), \widehat{\widetilde{m}}_s(-\omega), 0 \leq s \leq M-1$. Thus we may further assume that the displacement error satisfies the physical requirement (see [9] and [19])

$$0 \leq \epsilon < \frac{1}{2}. \tag{9}$$

A. (M, ϵ)-HRF is the low pass filter of a scaling function

Define $_{M,\epsilon}\phi$ by

$$_{M,\epsilon}\widehat{\phi}(\omega) = \prod_{k=1}^{\infty} {}_{M,\epsilon}\widehat{m}_0(M^{-k}\omega). \tag{10}$$

We first show that under the assumption of (9), the function $_{M,\epsilon}\phi$ defined in (10) is Hölder continuous and hence in $L^2(\mathbb{R})$. To this end, we notice that the (M, ϵ)-HRF can be decomposed into the sum of the filter $(\frac{1}{2} + \epsilon, \frac{1}{2} - \epsilon)$ with different shifts. For example, for $M = 2$, $\frac{1}{2}\left[\frac{1}{2} + \epsilon, 1, \frac{1}{2} - \epsilon\right] = \frac{1}{2}\left[\frac{1}{2} + \epsilon, \frac{1}{2} - \epsilon, 0\right] + \frac{1}{2}\left[0, \frac{1}{2} + \epsilon, \frac{1}{2} - \epsilon\right]$. In general, in the Fourier domain, we have

$$_{M,\epsilon}\widehat{m}_0(\omega) = \left[\left(\frac{1}{2} + \epsilon\right) + \left(\frac{1}{2} - \epsilon\right) e^{-j\omega}\right]$$
$$\times \frac{1}{M}\left[1 + e^{-j\omega} + \cdots + e^{-j(M-1)\omega}\right]. \tag{11}$$

Thus $_{M,\epsilon}\phi$ is supported in $[0, \frac{M}{M-1}] \subset [0, 2]$ and

$$\sum_{k \in \mathbb{Z}} {}_{M,\epsilon}\phi(x - k) = 1 \quad \forall \, x \in \mathbb{R} \tag{12}$$

([24], [25], [26]). Combining (5) and (12), we obtain

$$_{M,\epsilon}\phi\left(\frac{x}{M}\right) = \left(\frac{1}{2} + \epsilon\right) {}_{M,\epsilon}\phi(x),$$
$$_{M,\epsilon}\phi\left(\frac{x+1}{M}\right) = \left(\frac{1}{2} + \epsilon\right) + \left(\frac{1}{2} - \epsilon\right) {}_{M,\epsilon}\phi(x),$$
$$_{M,\epsilon}\phi\left(\frac{x+s}{M}\right) = 1 \quad \text{for } 2 \leq s \leq M-1,$$

where $x \in [0, 1)$. So $_{M,\epsilon}\phi$ is monotone on $[0, 1]$, and

$$|\,_{M,\epsilon}\phi(x) - \,_{M,\epsilon}\phi(y)| \leq C|x - y|^{\alpha_0}$$

for all $x, y \in \mathbb{R}$, where $\alpha_0 = -\frac{\ln \max(|\frac{1}{2} + \epsilon|, |\frac{1}{2} - \epsilon|)}{\ln M}$ and C is a positive constant ([30], [31]). Recall that $|\frac{1}{2} + \epsilon|, |\frac{1}{2} - \epsilon| < 1$ by (9). Then $_{M,\epsilon}\phi$ is Hölder continuous with Hölder exponent $\alpha_0 > 0$, and therefore belongs to $L^2(\mathbb{R})$.

For $\epsilon \in [0, \frac{1}{2})$, $\alpha_0 = -\frac{\ln|\frac{1}{2}+\epsilon|}{\ln M}$, which decreases as ϵ increases. Thus the scaling function $_{M,\epsilon}\phi$ becomes less smooth as ϵ increases, which can also be seen from the graphs of the scaling functions $_{M,\epsilon}\phi$ for $M = 2, 3, 4, 5$ in Figure 1. Also from those graphs, we observe that the functions $_{M,\epsilon}\phi$ are infinitely piecewise constant functions when $M \geq 3$. The theoretical proof of the above observation is given in [31] and [32].

Next, we show that the function $_{M,\epsilon}\phi$ is stable. It is known that $_{M,\epsilon}\phi$ is stable if and only if there exist two positive constants $0 < C_1 \leq C_2 < +\infty$ so that

$$C_1 \leq \sum_{k \in \mathbb{Z}} |_{M,\epsilon}\widehat{\phi}(\omega + 2k\pi)|^2 \leq C_2 \tag{13}$$

for all $\omega \in [-\pi, \pi]$ ([22], [24]). The estimate at the right hand side of (13) follows easily from the Poisson formula

$$\sum_{k \in \mathbb{Z}} |_{M,\epsilon}\widehat{\phi}(\omega + 2k\pi)|^2 = \sum_{l \in \mathbb{Z}} e^{-jl\omega} \int_{\mathbb{R}} {}_{M,\epsilon}\phi(x)\, {}_{M,\epsilon}\phi(x - l)dx,$$

and the fact that $_{M,\epsilon}\phi$ is a compactly supported L^2 function. On the other hand, the estimate at the left hand side of (13) is true since $_{M,\epsilon}\widehat{\phi}(\omega) \neq 0$ for all $\omega \in [-\pi, \pi]$, which follows from (10) and the observation that $_{M,\epsilon}\widehat{m}_0(\omega) \neq 0$ for all $\omega \in [-\frac{\pi}{M}, \frac{\pi}{M}]$ by (11). This proves the stability of $_{M,\epsilon}\phi$, and concludes that the filter $_{M,\epsilon}\widehat{m}_0$ is the low pass filter of the scaling function $_{M,\epsilon}\phi$.

Theorem 1: The function $_{M,\epsilon}\phi$ defined by (10) is a scaling function of a multiresolution analysis with dilation M, and the (M, ϵ)-HRF is the low pass filter associated with the scaling function $_{M,\epsilon}\phi$. Moreover, $_{M,\epsilon}\phi$ is supported in $\left[0, \frac{M}{M-1}\right]$, and Hölder continuous with Hölder exponent $\alpha_0 = -\frac{\ln \max(|\frac{1}{2}+\epsilon|,|\frac{1}{2}-\epsilon|)}{\ln M}$.

B. Dual low pass filters of the (M, ϵ)-HRF

In this subsection, we propose a constructive method to design the dual low pass filter $_{M,\epsilon}\widehat{\widetilde{m}}_0$ of $_{M,\epsilon}\widehat{m}_0$ so that

$$\sum_{t=0}^{M-1} {}_{M,\epsilon}\widehat{m}_0(\omega + \vartheta_t)\, {}_{M,\epsilon}\widehat{\widetilde{m}}_0^*(\omega + \vartheta_t) = 1 \quad \forall\, \omega \in \mathbb{R}, \tag{14}$$

and

$$_{M,\epsilon}\widehat{\widetilde{m}}_0(\vartheta_t) = 0 \quad \forall\, t = 1, \ldots, M - 1. \tag{15}$$

Also we discuss the construction of dual low pass filter with no displacement error.

By (11), we have $_{M,\epsilon}\widehat{m}_0(\omega) = {}_M\widehat{m}_0(\omega) + \frac{\epsilon}{M}(1 - e^{-jM\omega})$. This inspires us to construct $_{M,\epsilon}\widehat{\widetilde{m}}_0$ from $_M\widehat{\widetilde{m}}_0$, which is a solution of (14) and (15) with $\epsilon = 0$. Let

$$_{M,\epsilon}\widehat{\widetilde{m}}_0(\omega) = {}_M\widehat{\widetilde{m}}_0(\omega) + e^{-jk_0\omega}\widehat{m}(M\omega)$$

for some $\widehat{m}$, where $1 \leq k_0 \leq M - 1$. Substituting the above expression into (14) and (15), we obtain

$$\frac{\epsilon}{M}(1 - e^{-jM\omega}) \sum_{t=0}^{M-1} \widehat{\widetilde{m}}_0^*(\omega + \vartheta_t) + \widehat{m}^*(M\omega) = 0$$

and $\widehat{m}(0) = 0$. Therefore we have

Proposition 1: Assume that the sequence $_M\widetilde{m}_0$ is the dual low pass filter of $_M\widehat{m}_0$ for the case of no displacement error. Then

$$_{M,\epsilon}\widehat{\widetilde{m}}_0(\omega) := {}_M\widehat{\widetilde{m}}_0(\omega)$$
$$-e^{-jk_0\omega}\frac{\epsilon}{M}(1 - e^{jM\omega}) \sum_{t=0}^{M-1} \widehat{\widetilde{m}}_0(\omega + \vartheta_t) \tag{16}$$

is a dual low pass filter of $_{M,\epsilon}\widehat{m}_0$, where $1 \leq k_0 \leq M - 1$.

Notice that $\sum_{s=0}^{M-1} e^{-jk(\omega + \vartheta_s)} = Me^{-jk\omega}$ if k is a multiple of M; 0, otherwise. Thus the difference between $_{M,\epsilon}\widetilde{m}_0$ and $_M\widetilde{m}_0$ is $\epsilon[\,_M\widetilde{m}_0(kM) - \,_M\widetilde{m}_0((k+1)M)]$ occurring at indices $kM + k_0$ for possible k. For example, for $M = 2$,

$$_2\widehat{\widetilde{m}}_0(\omega) = -\frac{1}{8}e^{j\omega} + \frac{1}{4} + \frac{3}{4}e^{-j\omega} + \frac{1}{4}e^{-2j\omega} - \frac{1}{8}e^{-3j\omega}$$

is a dual low pass filter of $_2m_0$ [22]. Applying Proposition 1,

$$_{2,\epsilon}\widehat{\widetilde{m}}_0(\omega) = -\left(\frac{1}{8} - \frac{\epsilon}{4}\right)e^{j\omega} + \frac{1}{4} + \frac{3}{4}e^{-j\omega}$$
$$+\frac{1}{4}e^{-2j\omega} - \left(\frac{1}{8} + \frac{\epsilon}{4}\right)e^{-3j\omega} \tag{17}$$

is a dual low pass filter of $_2\widehat{m}_0$ ([19]).

Now we turn to discuss the construction of dual low pass filter with no displacement error. A filter $\widehat{m}$ is called interpolatory low pass filter if

$$\sum_{t=0}^{M-1} \widehat{m}(\omega + \vartheta_t) = 1 \quad \forall \ \omega \in \mathbb{R},$$

and

$$\widehat{m}(\vartheta_t) = \delta_{t,0}, \quad t = 0, \ldots, M - 1.$$

For the pair of the low pass filter $_M\widehat{m}_0$ and its dual low pass filter $_M\widehat{\widetilde{m}}_0$, the filter $\widehat{m}$ defined by

$$\widehat{m}(\omega) = \,_M\widehat{m}_0(\omega) \,_M\widehat{\widetilde{m}}_0^*(\omega),$$

is an interpolatory low pass filter, and satisfies

$$\widehat{m}(\vartheta_t) = \widehat{m}'(\vartheta_t) = 0, \quad t = 1, \ldots, M - 1. \tag{18}$$

Moreover,

$$\widehat{m}''(\pi) = 0 \tag{19}$$

if M is even, and

$$\widehat{m}(\pi) = 0 \tag{20}$$

if M is odd. It is known that any interpolatory low pass filter $\widehat{m}$, which satisfies (18), can be written as

$$\widehat{m}(\omega) = \frac{(1 - e^{jM\omega})(1 - e^{-jM\omega})}{M^2(1 - e^{j\omega})(1 - e^{-j\omega})}$$

$$+ (1 - e^{jM\omega})(1 - e^{-jM\omega}) \sum_{t=1}^{M-1} e^{-jt\omega} R_t(M\omega) \tag{21}$$

for some $R_t(\omega), 1 \le t \le M - 1$ ([33], [34], [35]). Substituting (21) into (19) and (20), we obtain

$$\sum_{t=1}^{M-1} (-1)^t R_t(M\pi) = -\frac{1}{4M^2}. \tag{22}$$

The general procedure to construct interpolatory low pass filters with preassigned zeros is discussed in [36] when $M = 2$. By (21) and (22), we get

Proposition 2: Let ${}_M\widehat{\widetilde{m}}_0$ be the dual low pass filter of ${}_M\widehat{m}_0$. Then

$${}_M\widehat{\widetilde{m}}_0(\omega) = \frac{1 - e^{-jM\omega}}{M - Me^{-j\omega}} \Big[\frac{1 + e^{-j\omega}}{2}$$

$$+ (1 - e^{-j\omega})(1 - e^{j\omega}) \frac{R(\omega) - R(\pi)}{1 + e^{j\omega}} \Big],$$

where R satisfies $R(\pi) = -\frac{1}{2}$ and $\sum_{t=0}^{M-1} R(\omega + \vartheta_t) = 0$.

In order to obtain a dual low pass filter ${}_M\widehat{\widetilde{m}}_0$ with minimal length, $\frac{R(\omega) - R(\pi)}{1 + e^{j\omega}}$ should be a constant, i.e., $R(\omega) = -\frac{1}{2} + c(1 + e^{j\omega})$. Since $\sum_{t=0}^{M-1} R(\omega + \vartheta_t) = 0$, it yields $c = \frac{1}{2}$. Thus, $R(\omega) = \frac{1}{2}e^{j\omega}$. By Proposition 2, we obtain the dual low pass filter ${}_M\widetilde{m}_0$ with minimal length,

$${}_M\widehat{\widetilde{m}}_0(\omega) = -\frac{1}{2M}e^{j\omega} + \frac{1}{M} + \cdots + \frac{1}{M}e^{-j(M-2)\omega}$$

$$+ \frac{3}{2M}e^{-j(M-1)\omega}.$$

Taking $k_0 = M - 1$ in Proposition 1 and using the above filter as the dual low pass filter with no

displacement error, we get a dual low pass filter $_{M,\epsilon}\widehat{\widetilde{m}}_0$ with minimal length and vanishing moment 1,

$$
\begin{aligned}
_{M,\epsilon}\widehat{\widetilde{m}}_0(\omega) &= \frac{1}{M}\left[1+\cdots+e^{-j(M-1)\omega}\right] \\
&\quad \times \left[-\left(\frac{1}{2}-\epsilon\right)e^{j\omega}+\left(\frac{3}{2}-\epsilon\right)\right] \\
&= -\left(\frac{1}{2M}-\frac{\epsilon}{M}\right)e^{j\omega}+\frac{1}{M}+\cdots \\
&\quad +\frac{1}{M}e^{-j(M-2)\omega}+\left(\frac{3}{2M}-\frac{\epsilon}{M}\right)e^{-j(M-1)\omega}.
\end{aligned}
\tag{23}
$$

For instance, the above dual low pass filter $_{M,\epsilon}\widehat{\widetilde{m}}_0$ becomes

$$
-\left(\frac{1}{4}-\frac{\epsilon}{2}\right)e^{j\omega}+\frac{1}{2}+\left(\frac{3}{4}-\frac{\epsilon}{2}\right)e^{-j\omega}
$$

when $M=2$,

$$
-\left(\frac{1}{6}-\frac{\epsilon}{3}\right)e^{j\omega}+\frac{1}{3}+\frac{1}{3}e^{-j\omega}+\left(\frac{1}{2}-\frac{\epsilon}{3}\right)e^{-2j\omega}
$$

when $M=3$, and

$$
-\left(\frac{1}{8}-\frac{\epsilon}{4}\right)e^{j\omega}+\frac{1}{4}+\frac{1}{4}e^{-j\omega}+\frac{1}{4}e^{-2j\omega}+\left(\frac{3}{8}-\frac{\epsilon}{4}\right)e^{-3j\omega}
$$

when $M=4$.

C. Dual low pass filter of a dual scaling function

In this subsection, we first show that the dual filter $_{M,\epsilon}\widehat{\widetilde{m}}_0(\omega)$ in (23) is the low pass filter associated with a multiresolution analysis with dilation M.

Theorem 2: Let either $M\geq 3$ and $\epsilon\in\left[0,\frac{1}{2}\right)$, or $M=2$ and $\epsilon\in\left(1-\frac{\sqrt{3}}{2},\frac{1}{2}\right)$, and let $_{M,\epsilon}\widetilde{\phi}$ be the solution of a refinement equation (5) with the symbol $_{M,\epsilon}\widehat{\widetilde{m}}_0$ in (23). Then $_{M,\epsilon}\widetilde{\phi}$ is a scaling function of a multiresolution analysis with dilation M.

Proof: We first prove the function $_{M,\epsilon}\widetilde{\phi}$, which is defined by

$$
_{M,\epsilon}\widehat{\widetilde{\phi}}(\omega) = \prod_{n=1}^{\infty} {}_{M,\epsilon}\widehat{\widetilde{m}}_0(M^{-n}\omega),
$$

is a function in $L^2(\mathbb{R})$. To this end, define the subdivision operator S corresponding to the low pass filter $_{M,\epsilon}\widehat{m}_0$ by

$$
Su(k) = \sum_{k'\in\mathbb{Z}} {}_{M,\epsilon}m_0(k-Mk')u(k),\ k\in\mathbb{Z},
$$

where $u := \{u(k)\}$. By calculation, the Fourier series of the sequence $\nabla S^n \delta$ is

$$\left(1 - e^{-jM^n\omega}\right) \prod_{i=0}^{n-1} \left(-\left(\frac{1}{2} - \epsilon\right) e^{jM^i\omega} + \left(\frac{3}{2} - \epsilon\right) \right)$$

for any $n \geq 1$, where δ is the usual delta sequence. Thus

$$\begin{aligned}
\|\nabla S^n \delta\|_2^2 &= 2\left(\left(\frac{1}{2} - \epsilon\right)^2 + \left(\frac{3}{2} - \epsilon\right)^2 \right)^n \\
&= 2\left(\frac{1}{2} + 2(1 - \epsilon)^2 \right)^n,
\end{aligned}$$

which implies that

$$\|\nabla S^n \delta\|_2^2 \leq 2M^n \quad \forall \, n \geq 1,$$

for either $M \geq 3$ and $\epsilon \in \left[0, \frac{1}{2}\right)$, or $M = 2$ and $\epsilon \in \left(1 - \frac{\sqrt{3}}{2}, \frac{1}{2}\right)$. Thus $_{M,\epsilon}\widetilde{\phi}$ is a function in $L^2(\mathbb{R})$ ([24], [37]). Following the proof of Theorem 1 leads to the stability of $_{M,\epsilon}\phi$. $\square$

The dual scaling functions $_{M,\epsilon}\widetilde{\phi}$ for $M = 3, 4, 5$ are shown in Figure 2. The dual scaling functions $_{M,\epsilon}\widetilde{\phi}$ are not Hölder continuous. In particular, the Hölder exponent of the dual scaling functions $_{M,\epsilon}\widetilde{\phi}$ is $-\frac{\ln(\frac{3}{2} - \epsilon)}{\ln M}$ and thus negative for any $\epsilon \in [0, \frac{1}{2})$. But as seen from the graphs, the dual scaling functions $_{M,\epsilon}\widetilde{\phi}$ becomes less irregular as ϵ increases.

The rest of this section is devoted to show that the pair of scaling functions $_{M,\epsilon}\phi$ and $_{M,\epsilon}\widetilde{\phi}$ is a dual pair, where the symbols of the scaling functions $_{M,\epsilon}\phi$ and $_{M,\epsilon}\widetilde{\phi}$ are defined as in (11) and (23) respectively. Our result is the following:

Theorem 3: Let $_{M,\epsilon}\phi$ and $_{M,\epsilon}\widetilde{\phi}$ be the scaling functions with their corresponding low pass filters as in (11) and (23) respectively. Assume that either $M \geq 3$ and $\epsilon \in (0, \frac{1}{2})$, or $M = 2$ and $\epsilon \in \left(1 - \frac{\sqrt{3}}{2}, \frac{1}{2}\right)$. Then $_{M,\epsilon}\widetilde{\phi}$ is the dual of $_{M,\epsilon}\phi$.

Proof: Let $\widehat{m}(\omega) := {_{M,\epsilon}\widehat{m}_0(\omega)} \, {_{M,\epsilon}\widehat{\widetilde{m}}_0^*(\omega)}$, and let $_{M,\epsilon}\Phi$ be the solution of the refinement equation (5) with symbol $\widehat{m}$. Clearly $\widehat{m}$ is an interpolatory low pass filter, and

$$_{M,\epsilon}\widehat{\Phi}(\omega) = {_{M,\epsilon}\widehat{\phi}(\omega)} \, {_{M,\epsilon}\widehat{\widetilde{\phi}}^*(\omega)}.$$

By Theorems 1 and 2, both $_{M,\epsilon}\phi$ and $_{M,\epsilon}\widetilde{\phi}$ are compactly supported functions in L^2, and hence $_{M,\epsilon}\Phi$ is a compactly supported continuous function. By (11) and (23), both $_{M,\epsilon}\widehat{m}_0(\omega)$ and $_{M,\epsilon}\widehat{\widetilde{m}}_0(\omega)$ are nonzero for all $\omega \in \left[-\frac{\pi}{M}, \frac{\pi}{M}\right]$. Thus the stability of $_{M,\epsilon}\Phi$ follows by the same procedure as used in the proof of Theorem 1. Therefore $_{M,\epsilon}\Phi$ satisfies interpolatory condition, that is, $_{M,\epsilon}\Phi(k) = \delta_{k,0}, \quad k \in \mathbb{Z}$ ([24], [33], [38]). This proves the dual property between $_{M,\epsilon}\phi$ and $_{M,\epsilon}\widetilde{\phi}$. $\square$

Remark: For $M = 2$, if the displacement error $0 \leq \epsilon \leq 1 - \frac{\sqrt{3}}{2}$, we can use the dual filter (17) instead of the one in (23) to obtain a dual scaling function in $L^2(\mathbb{R})$.

IV. BI-ORTHOGONAL WAVELET FILTER BANK

In this section, we consider the construction of bi-orthogonal wavelet filter bank with low pass filter and the dual low pass filter given in (11) and (23), that is, to find high pass filters $_{M,\epsilon}\widehat{m}_t, 1 \leq t \leq M-1$, and dual high pass filters $_{M,\epsilon}\widehat{\widetilde{m}}_t, 1 \leq t \leq M-1$, so that

$$\sum_{s=0}^{M-1} {}_{M,\epsilon}\widehat{m}_t(\omega + \vartheta_s) \, {}_{M,\epsilon}\widehat{\widetilde{m}}_{t'}^{*}(\omega + \vartheta_s) = \delta_{t,t'} \tag{24}$$

for all $t, t' = 0, \ldots, M-1$, and

$$_{M,\epsilon}\widehat{m}_t(0) = {}_{M,\epsilon}\widehat{\widetilde{m}}_t(0) = 0 \tag{25}$$

for $t = 1, \ldots, M-1$.

The equation (25) follows from taking $\omega = 0$ in (24) and using the low pass filter properties of the filters $_{M,\epsilon}\widehat{m}_0$ and $_{M,\epsilon}\widehat{\widetilde{m}}_0$. To solve the equation (24), we need the polyphase decomposition of the filters $_{M,\epsilon}\widehat{m}_t$ and $_{M,\epsilon}\widehat{\widetilde{m}}_t, 0 \leq t \leq M-1$. Let

$$_{M,\epsilon}\widehat{m}_t(\omega) = \sum_{s=0}^{M-1} e^{-js\omega} \, {}_{M,\epsilon}\widehat{m}_{t,s}(M\omega) \tag{26}$$

for $0 \leq t \leq M-1$, and set

$$\mathbf{H}(\omega) = \begin{bmatrix} {}_{M,\epsilon}\widehat{m}_{0,0}(\omega) & \cdots & {}_{M,\epsilon}\widehat{m}_{0,M-1}(\omega) \\ \vdots & \ddots & \vdots \\ {}_{M,\epsilon}\widehat{m}_{M-1,0}(\omega) & \cdots & {}_{M,\epsilon}\widehat{m}_{M-1,M-1}(\omega) \end{bmatrix}. \tag{27}$$

Similarly let

$$_{M,\epsilon}\widehat{\widetilde{m}}_t(\omega) = \sum_{s=0}^{M-1} e^{-js\omega} \, {}_{M,\epsilon}\widehat{\widetilde{m}}_{t,s}(M\omega) \tag{28}$$

and set

$$\widetilde{\mathbf{H}}(\omega) = \begin{bmatrix} {}_{M,\epsilon}\widehat{\widetilde{m}}_{0,0}(\omega) & \cdots & {}_{M,\epsilon}\widehat{\widetilde{m}}_{0,M-1}(\omega) \\ \vdots & \ddots & \vdots \\ {}_{M,\epsilon}\widehat{\widetilde{m}}_{M-1,0}(\omega) & \cdots & {}_{M,\epsilon}\widehat{\widetilde{m}}_{M-1,M-1}(\omega) \end{bmatrix}. \tag{29}$$

Then we may write (24) as

$$\mathbf{H}(\omega)\widetilde{\mathbf{H}}(-\omega)^T = \frac{1}{M}\mathbf{I}. \tag{30}$$

By (11) and (23), the first row of $\mathbf{H}$ is

$$\mathbf{a}_0 + \mathbf{b}_0 e^{-j\omega} := \frac{1}{M}\left[\left(\frac{1}{2} + \epsilon\right) + \left(\frac{1}{2} - \epsilon\right)e^{-j\omega}, 1, \cdots, 1\right],$$

and the one of $\widetilde{\mathbf{H}}$ is

$$\widetilde{\mathbf{a}}_0 + \widetilde{\mathbf{b}}_0 e^{j\omega} := \frac{1}{M}\left[1, \cdots, 1, \left(\frac{3}{2} - \epsilon\right) - \left(\frac{1}{2} - \epsilon\right)e^{j\omega}\right].$$

We do not intend to find all solutions of the equation (30) (see [28], [29] for general results), but here we try to find some solutions of the form

$$\mathbf{H}(\omega) = \mathbf{H}_1 + \mathbf{H}_2 e^{-j\omega} \tag{31}$$

and

$$\widetilde{\mathbf{H}}(\omega) = \widetilde{\mathbf{H}}_1 + \widetilde{\mathbf{H}}_2 e^{j\omega}, \tag{32}$$

where $\mathbf{H}_1, \mathbf{H}_2, \widetilde{\mathbf{H}}_1$ and $\widetilde{\mathbf{H}}_2$ are square matrices with real entries.

For $M = 2$, one may verify that

$$\mathbf{H}(\omega) = \frac{1}{2}\begin{bmatrix} \frac{1}{2} + \epsilon & 1 \\ -\frac{3}{2} + \epsilon & 1 \end{bmatrix} + \frac{1}{2}\begin{bmatrix} \frac{1}{2} - \epsilon & 0 \\ \frac{1}{2} - \epsilon & 0 \end{bmatrix} e^{-j\omega}$$

and

$$\widetilde{\mathbf{H}}(\omega) = \frac{1}{2}\begin{bmatrix} 1 & \frac{3}{2} - \epsilon \\ -1 & \frac{1}{2} + \epsilon \end{bmatrix} + \frac{1}{2}\begin{bmatrix} 0 & -\frac{1}{2} + \epsilon \\ 0 & \frac{1}{2} - \epsilon \end{bmatrix} e^{j\omega}$$

satisfies (30). Therefore

$$_{2,\epsilon}\widehat{m}_1(\omega) = \frac{1}{2}\left[-\left(\frac{3}{2} - \epsilon\right) + e^{-j\omega} + \left(\frac{1}{2} - \epsilon\right)e^{-2j\omega}\right] \tag{33}$$

and

$$_{2,\epsilon}\widehat{\widetilde{m}}_1(\omega) = \frac{1}{2}\left[\left(\frac{1}{2} - \epsilon\right)e^{j\omega} - 1 + \left(\frac{1}{2} + \epsilon\right)e^{-j\omega}\right] \tag{34}$$

are the high pass filter and dual high pass filter corresponding to the low pass filter $_{2,\epsilon}\widehat{m}_0$ and the dual pass filter $_{2,\epsilon}\widehat{\widetilde{m}}_0$ (see Table I for the filter coefficients).

For $M \geq 3$, we start from an $(M - 2) \times (M - 2)$ square matrix $\mathbf{A}$ so that

$$\mathbf{A}\mathbf{A}^T = \mathbf{I} \tag{35}$$

and

$$\text{the first row of } \mathbf{A} \text{ is } \frac{1}{\sqrt{M-2}}[1, \ldots, 1]. \tag{36}$$

Define

$$\mathbf{H}(\omega) = \frac{1}{M} \begin{bmatrix} 2-\theta & \sqrt{M-2} & \mathbf{0} & 1 \\ -\sqrt{M-2} & 1 & \mathbf{0} & 0 \\ \mathbf{0} & \mathbf{0} & \sqrt{M}\mathbf{I}_{M-3} & \mathbf{0} \\ -\theta & 0 & \mathbf{0} & 1 \end{bmatrix}$$
$$\times \begin{bmatrix} 1 & \mathbf{0} & 0 \\ \mathbf{0} & \mathbf{A} & \mathbf{0} \\ 0 & \mathbf{0} & 1 \end{bmatrix}. \tag{37}$$

and

$$\widetilde{\mathbf{H}}(-\omega) = \frac{1}{M}$$
$$\begin{bmatrix} 1 & \sqrt{M-2} & \mathbf{0} & \theta \\ -\sqrt{M-2} & 2 & \mathbf{0} & -\sqrt{M-2}\theta \\ \mathbf{0} & \mathbf{0} & \sqrt{M}\mathbf{I}_{M-3} & \mathbf{0} \\ -1 & -\sqrt{M-2} & \mathbf{0} & M-\theta \end{bmatrix}$$
$$\times \begin{bmatrix} 1 & \mathbf{0} & 0 \\ \mathbf{0} & \mathbf{A} & \mathbf{0} \\ 0 & \mathbf{0} & 1 \end{bmatrix}, \tag{38}$$

where

$$\theta = \left(\frac{3}{2} - \epsilon\right) - \left(\frac{1}{2} - \epsilon\right) e^{-j\omega}.$$

Clearly, $\mathbf{H}$ has the form (31) and its first row is $\mathbf{a}_0 + \mathbf{b}_0 e^{-j\omega}$. Similarly $\widetilde{\mathbf{H}}$ has the form (32) and its first row is $\widetilde{\mathbf{a}}_0 + \widetilde{\mathbf{b}}_0 e^{j\omega}$. By simply calculation, we may verify that the matrices $\mathbf{H}$ and $\widetilde{\mathbf{H}}$ in (37) and (38) satisfy (30).

For $M = 3$, the only matrix $\mathbf{A}$ in (35) and (36) is the number 1. Thus the corresponding filter coefficients for the bi-orthogonal wavelet filter bank are as given in Table II.

For $M = 4$, the matrix $\mathbf{A} = \frac{1}{\sqrt{2}} \begin{bmatrix} 1 & 1 \\ 1 & -1 \end{bmatrix}$ satisfies (35) and (36). The corresponding filter coefficients of the bi-orthogonal wavelet filter bank are as given in Table III.

V. Numerical experiments

In this section, we implement the high-resolution image reconstruction algorithm (4) using the bi-orthogonal wavelet filters constructed in the previous sections. We use the "Boat" and "Bridge" images of size 260×260 shown in Fig. 3 as the original images in the numerical tests. We abbreviate the

least-square method (see [21]), the wavelet method with the dual filter (17) (see [19]), and the wavelet method with the dual filter in Tables I, II, III by LSM, WAD, WAM respectively. The periodic boundary condition [21] is used for all the methods.

In the first test, we use a 2×2 sensor array with no displacement error, and with displacement error $\epsilon = \epsilon^x_{m_1,m_2} = \epsilon^y_{m_1,m_2} = \frac{1}{4}$, $m_1, m_2 \in \{0,1\}$. Those sense arrays produce four low-resolution images which are corrupted by white Gaussian noise with different signal-to-noise ratio (SNR). Table IV gives the PSNR results of the image obtained by LSM, WAD and WAM, while Figs. 4 and 5 depict the reconstructed high-resolution images for the "Boat" and "Bridge" images with noise at SNR=30 dB and displacement error $\epsilon = \frac{1}{4}$. From the above table and figures we see that the wavelet algorithm (WAM, WAD) performs better than the least square method (LSM) does. We also have two interested observations related to the displacement error. From the Table IV, we see that WAD works better than WAM in the sense of PSNR when there is no displacement error, and that WAM performs better than WAD when the displacement error is $\frac{1}{4}$. We think that it is because when $|\epsilon| \leq 1 - \frac{\sqrt{3}}{2}$, the corresponding scaling function $_{M,\epsilon}\widetilde{\phi}$ to the dual low pass filter in Table I is not in L^2 and hence is too irregular. A careful comparison in the Figs. 4 and 5 reveals that the reconstructed images Fig. 4(d) and Fig. 5(d) with the minimally supported dual filter in Table I have less artifacts than that of Fig. 4(c) and Fig. 5(c) with the dual filter in (17).

In the second test, a 3×3 sensor array with no displacement error and with displacement error $\epsilon^x_{m_1,m_2} = \epsilon^y_{m_1,m_2} = \frac{1}{4}$, $m_1, m_2 \in \{0,1,2\}$, are considered. In this test, we use the wavelet-based iterative algorithm (4) with the wavelet filter coefficients in Table II for the high-resolution image reconstruction. Table V gives the PSNR results for the least-square method and the wavelet method with the dual filter in Table II, while Fig. 6 depicts the reconstructed high-resolution images for the "Boat" and "Bridge" images for the case with displacement error $\frac{1}{4}$. Similar to the first test, the wavelet-based algorithm shows improvement over the least square method in both image quality and PSNR, and also the image quality improves as the displacement error changes from 0 to $\frac{1}{4}$. We believe that the image quality improvement comes also from the change of the regularity of the dual scaling function $_{M,\epsilon}\widetilde{\phi}$ as the displacement error changes from 0 to $\frac{1}{4}$.

In the third test, we have done similar test as the first test. A 4×4 sensor array with no displacement error and with displacement error $\epsilon^x_{m_1,m_2} = \epsilon^y_{m_1,m_2} = \frac{1}{4}$, $m_1, m_2 \in \{0,1,2,3\}$, are considered. We use the wavelet-based iterative algorithm (4) with the wavelet filter coefficients in Table III for the high-resolution image reconstruction. Table VI gives the PSNR results of the image obtained by LSM, WAD and WAM, while Fig. 7 depicts the partial reconstructed high-resolution images for the "Bridge" images

with noise at SNR=30 dB and displacement error $\epsilon = \frac{1}{4}$. We can see that our proposed wavelet-based algorithms give better denoising performance than LSM.

In the forth test, we let the 4×4 sensor array have displacement error

$$\epsilon^x = \begin{bmatrix} 0.1548 & 0.0984 & 0.0242 & 0.0607 \\ 0.0843 & 0.2317 & 0.0535 & 0.1590 \\ 0.1952 & 0.1873 & 0.1892 & 0.1141 \\ 0.0054 & 0.1428 & 0.1491 & 0.2194 \end{bmatrix}$$

and

$$\epsilon^y = \begin{bmatrix} 0.2043 & 0.0021 & 0.0074 & 0.0904 \\ 0.1759 & 0.1693 & 0.1266 & 0.0302 \\ 0.2351 & 0.1742 & 0.0829 & 0.1671 \\ 0.1953 & 0.0071 & 0.0075 & 0.0840 \end{bmatrix},$$

and use the coefficients of the bi-orthogonal wavelet filter bank in Table III. The low-resolution 64×64 frames from $(0,0)$th sensor are shown in Figs. 8(a) and (b) for the "Boat" image and "Bridge" image respectively. Accordingly, the observed high-resolution images with white Gaussian noise SNR of 30 dB are shown in Figs. 8(c) and (d), and the reconstructed high-resolution images are shown in Figs. 8 (e) and (f). The values of PSNR with LSM and WAM for "Boat" image are respectively 24.96 dB and 27.37 dB while The values of PSNR with LSM and WAM for "Bridge" image are respectively 23.93 dB and 24.03 dB. Again, we can see that the wavelet-based algorithm works better than the least-square method in the sense of PSNR.

VI. Conclusions

The high-resolution filter (M, ϵ)-HRF (1) is formulated from the mathematical model for high-resolution image reconstruction ([9]), where $M \geq 2$ is the resolution ratio and $\epsilon \in (-\frac{1}{2}, \frac{1}{2})$ is the displacement error of the sensors. In this paper, we first observe that the high-resolution filter (M, ϵ)-HRF is the low pass filter of a multiresolution analysis (Theorem 1); Then we construct the minimally supported bi-orthogonal wavelet system, whose primal low pass filter is the (M, ϵ)-HRF, explicitly (Theorems 2 and 3, and Section IV); Finally we introduce a wavelet-based iterative algorithm (4) and do some numerical experiments. From our numerical experiments, the iterative algorithm corresponding to the bi-orthogonal wavelet system designed in this paper shows improvement over the common-used least square method (see for instance [21]) in output image quality and PSNR, and over the similar wavelet-based algorithm with different wavelet filters ([19]) in less artifacts.

REFERENCES

[1] T. Huang and R. Tsay, "Multiple frame image restoration and registration," in *Advances in Computer Vision and Image Processing*, T. S. Huang, Ed., vol. 1, Greenwich, CT: JAI, 1984, pp. 317–339.

[2] S. P. Kim, N. K. Bose, and H. M. Vakenzuela, "Recursive reconstruction of high resolution image from noisy undersampled multiframes," *IEEE Transactions on Acoustics, Speech, and Signal Processing*, vol. 38, pp. 1013–1027, June 1990.

[3] A. Tekalp, T. Ozkan, and M. Sezan, "High resolution image reconstruction from low-resolution image sequences, and space varying image restoration," in *IEEE Int. Conf. Acoustics, Speech, Signal Processing*, vol. 3, San Francisco, CA, Mar. 1992, pp. 169–172.

[4] J. C. Gillete, T. M. Stadtmiller, and R. C. Hardie, "Aliasing reduction in starting infrared images utilizing subpixel techniques," *Optical Engineering*, vol. 34, no. 11, p. 3130, Nov. 1995.

[5] R. Schultz and R. Stevenson, "Extraction of high-resolution frames from video sequences," *IEEE Transactions on Image Processing*, vol. 5, pp. 996–1011, June 1996.

[6] M. Elad and A. Feuer, "Restoration of a single superresolution image from several blurred, noisy and undersampled measured images," *IEEE Transactions on Image Processing*, vol. 6, pp. 1646–1658, Dec. 1997.

[7] R. Hardie, K. Barnard, and E. Armstrong, "Joint MAP registration and high-resolution image estimation using a sequence of undersampled images," *IEEE Trans. on Image Processing*, vol. 6, pp. 1621–1633, 1997.

[8] A. Patti, M. Sezan, and A. Tekalp, "Superresolution video reconstruction with arbitrary sampling lattices and nonzero aperture time," *IEEE Transactions on Image Processing*, vol. 6, pp. 1064–1076, Aug. 1997.

[9] N. Bose and K. Boo, "High-resolution image reconstruction with multisensors," *International Journal of Imaging Systems and Technology*, vol. 9, pp. 294–304, 1998.

[10] M. Elad and A. Feuer, "Superresolution restoration of an image sequence: adaptive filtering approach," *IEEE Transactions on Image Processing*, vol. 8, no. 3, pp. 387–395, Mar. 1999.

[11] M. Ng, R. Chan, T. Chan, and A. Yip, "Cosine transform preconditioners for high resolution image reconstruction," *Linear Algebra and its Applications*, vol. 316, pp. 89–104, 2000.

[12] N. Nguyen, P. Milanfar, and G. Golub, "A computationally efficient superresolution image reconstruction algorithm," *IEEE Trans. on Image Processing*, vol. 10, pp. 573–583, 2001.

[13] B. Tom, N. Galatsanos, and A. Katsaggelos, *Reconstruction of a high-resolution image from multiple low resolution images*, ser. Super-Resolution Imaging. Kluwer Academic Publisher, 2001, ch. 4, pp. 73–105.

[14] M. Ng and A. Yip, "A fast MAP algorithm for high-resolution image reconstruction with multisensors," *Multidimensional Systems and Signal Processing*, vol. 12, pp. 143–164, 2001.

[15] M. K. Ng and N. Bose, "Analysis of displacement errors in high-resolution image reconstruction with multisensors," *IEEE Trans. on Circuits and Systems—I: Fundamental Theory and Applications*, vol. 49, no. 6, pp. 806–813, 2002.

[16] M. K. Ng, J. Koo, and N. Bose, "Constrained total least squares computations for high resolution image reconstruction with multisensors," *International Journal of Imaging Systems and Technology*, vol. 12, pp. 35–42, 2002.

[17] R. Molina, M. Vega, J. Abad, and A. Katsaggelos, "Parameter estimation in bayesian high-resolution image reconstruction with multisensors," Tech. Rep., Oct. 2002.

[18] R. Chan, T. Chan, L. Shen, and Z. Shen, "Wavelet algorithms for high-resolution image reconstruction," *SIAM Journal on Scientific Computing*, vol. 24, no. 4, pp. 1408–1432, 2003.

[19] ——, "Wavelet deblurring algorithms for spatially varying blur from high-resolution image reconstruction," *Linear Algebra and its Applications*, vol. 366, pp. 139–155, 2003.

[20] D. Donoho and I. Johnstone, "Ideal spatial adaptation by wavelet shrinkage," *Biometrika*, vol. 81, pp. 425–455, 1994.

[21] R. Gonzalez and R. Woods, *Digital Image Processing*.   Addison-Wesley, 1993.

[22] I. Daubechies, *Ten Lectures on Wavelets*, ser. CBMS Conference Series in Applied Mathematics.   Philadelphia: SIAM, 1992, vol. 61.

[23] S. Mallat, *A Wavelet Tour of Signal Processing*, 2nd ed.   Academic Press, 1999.

[24] Q. Sun, N. Bi, and D. Huang, *An Introduction to Multi-band Wavelets*.   Zhejiang University Press, 2001.

[25] G. Strang and T. Q. Nguyen, *Wavelets and Filterbanks*.   Wellesley, MA: Wellesley-Cambridge, 1997.

[26] P. Vaidyanathan, *Multirate Systems and Filter Banks*.   New Jersey: Prentice Hall, Englewood Cliffs, 1993.

[27] P. Soardi, "Biorthogonal M-channel compactly supported wavelets," *Constr. Approximation*, vol. 16, pp. 283–311, 2000.

[28] Z. Shen, "Extension of matrices with Laurent polynomial entries," in Proceedings of the 15th IMACS World Congress on Scientific Computation Modeling and Applied Mathematics, Ashim Syclow eds., vol. 1, 1997, pp. 57–61.

[29] W. Lawton, S. Lee, and Z. Shen, "An algorithm for matrix extension and wavelet construction," *Math. Computation*, vol. 65, pp. 723–737, 1996.

[30] I. Daubechies and J. C. Lagaris, "Two-scale difference equations I: Existence and global regularity of solutions," *SIAM J. Math. Anal.*, vol. 22, no. 5, pp. 1399–1410, 1991.

[31] Q. Sun and Z. Zhang, "M-band scaling function with filter having vanishing moments two and minimal length," *J. Math. Anal. Appl.*, vol. 222, pp. 225–243, 1998.

[32] X. Dai, D. Huang, and Q. Sun, "Local polynomial property and linear independence of refinable distributions," *Archiv Math.*, vol. 78, pp. 74–80, 2002.

[33] N. Bi, X. Dai, and Q. Sun, "Construction of compactly supported M-band wavelets," *Applied and Computational Harmonic Analysis*, vol. 6, pp. 113–131, 1999.

[34] Z. Shi, G. W. Wei, D. Kouri, D. Hoffman, and Z. Bao, "Lagrange wavelets for signal processing," *IEEE Transactions on Image Processing*, vol. 10, no. 10, pp. 1488–1508, 2001.

[35] P. Heller, "Rank M wavelets with N vanishing moments," *SIAM J. Matrix Analysis and Its Applications*, vol. 16, pp. 502–519, 1995.

[36] C. Micchelli, "On a family of filters arising in wavelet construction," *Applied and Computational Harmonic Analysis*, vol. 4, pp. 38–50, 1997.

[37] R.-Q. Jia, "Characterization of smoothness of multivariate refinable functions in Sobolev space," *Transaction of American Mathematical Society*, vol. 351, pp. 4089–4112, 1999.

[38] R. Lewis, "Cardinal interpolation multiresolution," *Journal of Approximation Theory*, vol. 26, pp. 177–202, 1994.

Lixin Shen received his BSc and MSc from Peking University, China, in 1987 and 1990, respectively, and his PhD degree from Zhongshan University, China, in 1996, all in mathematics. From September 1996 to July 2001, he was a research fellow at Center for Wavelets, Approximation, and Information Processing, National University of Singapore. From August 2001 to July 2002, he was a post-doctoral fellow at Virtual Environments Research Institute, University of Houston. He is currently a Research Assistant Professor at the Department of Mathematics, West Virginia University. His current research interests are wavelets and their application in image processing.

Qiyu Sun received the BSc and PhD degree in mathematics from Hangzhou University, China in 1985,1990 respectively. He is currently visiting University of Houston. His prior position was with the Zhejiang University, China, the National University of Singapore, Singapore, and Vanderbilt University. His research interest includes multi-band wavelets, shift-invariant spaces, wavelet and framelet theory, sampling theory, and Fourier analysis. He has published more than 60 papers and written a book "An Introduction to Multiband Wavelets" with Ning Bi and Daren Huang. He is the guest editor of the Special Issue on Frames (2003) of the journal of Advance in Computational Mathematics.

Figure Captions

Figure 1. The plots of the scaling function $_{M,\epsilon}\phi$ with $\epsilon = 0$ (left column) and $\epsilon = \frac{1}{4}$ (right column) corresponding to $_{M,\epsilon}m_0$ with $M = 2, 3, 4, 5$ (from top to bottom).

Figure 2. The plots of the dual scaling function $_{M,\epsilon}\widetilde{\phi}$ with $\epsilon = 0$ (left column) and $\epsilon = \frac{1}{4}$ (right column) corresponding to $_{M,\epsilon}\widetilde{m}_0$ with $M = 3, 4, 5$ (from top to bottom).

Figure 3. (a) The original "Boat" image; (b) The original "Bridge" image.

Figure 4. Numerical result for "Boat" image with displacement error $\frac{1}{4}$: (a) Observed high-resolution 256×256 image (with white noise at SNR=30dB added); (b) Reconstructed 256×256 image from LSM; (c) Reconstructed 256×256 image from WAD; (d) Reconstructed 256×256 image from WAM.

Figure 5. Numerical result for "Bridge" image with displacement error $\frac{1}{4}$: (a) Observed high-resolution 256×256 image (with white noise at SNR=30dB added); (b) Reconstructed 256×256 image from LSM; (c) Reconstructed 256×256 image from WAD; (d) Reconstructed 256×256 image from WAM.

Figure 6. For the case with displacement error $\frac{1}{4}$, the images (from top to bottom) are observed high-resolution 256×256 images, reconstructed high-resolution images from LSM, and reconstructed high-resolution images from WAM, respectively. The left column is for "Boat" image, while the right column is for "Bridge" image.

Figure 7. Zoom of numerical result for "Bridge" image with displacement error $\epsilon = \frac{1}{4}$: (a) Original high-resolution; (b) Reconstructed image from LSM; (c) Reconstructed image from WAD; (d) Reconstructed image from WAM.

Figure 8. The images (from top to bottom) are the low-resolution 64×64 images from the $(0,0)$th sensor, reconstructed high-resolution images from LSM, and reconstructed high-resolution images from WAM, respectively. The left column is for "Boat" images, while the right column is for "Bridge" images.

Table Captions

Table I The coefficients of the bi-orthogonal wavelet filter bank for $M = 2$ and $\epsilon \in \left(1 - \frac{\sqrt{3}}{2}, \frac{1}{2}\right)$.

Table II The coefficients of the bi-orthogonal wavelet filter bank for $M = 3$ and $\epsilon \in [0, \frac{1}{2})$, where $\delta_1 = \frac{1}{6} - \frac{\epsilon}{3}$ and $\delta_2 = \frac{1}{2} - \frac{\epsilon}{3}$.

Table III The coefficients of the bi-orthogonal wavelet filter bank for $M = 4$ and $\epsilon \in [0, \frac{1}{2})$, where $\delta_3 = \frac{1}{8} - \frac{\epsilon}{4}$.

Table IV The PSNR results for the 2×2 sensor array.

Table V The PSNR results for the 3×3 sensor array.

Table VI The PSNR results for the 4×4 sensor array.

k	$_{2,\epsilon}m_0$	$_{2,\epsilon}m_1$	$_{2,\epsilon}\widetilde{m}_0$	$_{2,\epsilon}\widetilde{m}_1$
-1			$-\frac{1}{4}+\frac{\epsilon}{4}$	$\frac{1}{4}-\frac{\epsilon}{2}$
0	$\frac{1}{4}+\frac{\epsilon}{2}$	$-\frac{3}{4}+\frac{\epsilon}{2}$	$\frac{1}{2}$	$-\frac{1}{2}$
1	$\frac{1}{2}$	$\frac{1}{2}$	$\frac{3}{4}-\frac{\epsilon}{2}$	$\frac{1}{4}+\frac{\epsilon}{2}$
2	$\frac{1}{4}-\frac{\epsilon}{2}$	$\frac{1}{4}-\frac{\epsilon}{2}$		

Table 1

p	$_{3,\epsilon}m_0$	$_{3,\epsilon}m_1$	$_{3,\epsilon}m_2$	$_{3,\epsilon}\widetilde{m}_0$	$_{3,\epsilon}\widetilde{m}_1$	$_{3,\epsilon}\widetilde{m}_2$
-1				$-\delta_1$	δ_1	δ_1
0	$\frac{1}{3}-\delta_1$	$-\frac{1}{3}$	$-\delta_2$	$\frac{1}{3}$	$-\frac{1}{3}$	$-\frac{1}{3}$
1	$\frac{1}{3}$	$\frac{1}{3}$	0	$\frac{1}{3}$	$\frac{2}{3}$	$-\frac{1}{3}$
2	$\frac{1}{3}$	0	$\frac{1}{3}$	δ_2	$-\delta_2$	$1-\delta_2$
3	δ_1	0	δ_1			

Table 2

p	$_{4,\epsilon}m_0$	$_{4,\epsilon}m_1$	$_{4,\epsilon}m_2$	$_{4,\epsilon}m_3$
0	$\frac{1}{4} - \delta_3$	$-\frac{\sqrt{2}}{4}$	0	$-\frac{1}{4} - \delta_3$
1	$\frac{1}{4}$	$\frac{\sqrt{2}}{8}$	$\frac{\sqrt{2}}{4}$	0
2	$\frac{1}{4}$	$\frac{\sqrt{2}}{8}$	$-\frac{\sqrt{2}}{4}$	0
3	$\frac{1}{4}$	0	0	$\frac{1}{4}$
4	δ_3	0	0	δ_3

p	$_{4,\epsilon}\widetilde{m}_0$	$_{4,\epsilon}\widetilde{m}_1$	$_{4,\epsilon}\widetilde{m}_2$	$_{4,\epsilon}\widetilde{m}_3$
-1	$-\delta_3$	$\sqrt{2}\delta_3$	0	δ_3
0	$\frac{1}{4}$	$-\frac{\sqrt{2}}{4}$	0	$-\frac{1}{4}$
1	$\frac{1}{4}$	$\frac{\sqrt{2}}{4}$	$\frac{\sqrt{2}}{4}$	$-\frac{1}{4}$
2	$\frac{1}{4}$	$\frac{\sqrt{2}}{4}$	$-\frac{\sqrt{2}}{4}$	$-\frac{1}{4}$
3	$\frac{1}{4} + \delta_3$	$-\frac{\sqrt{2}}{4} - \sqrt{2}\delta_3$	0	$\frac{3}{4} - \delta_3$

Table 3

Image	SNR	$\epsilon = 0$			$\epsilon = \frac{1}{4}$		
		LSM	WAD	WAM	LSM	WAD	WAM
	20	29.15	32.04	31.55	28.32	31.28	31.12
Boat	30	30.02	32.68	32.13	29.09	31.85	32.65
	40	30.40	32.93	32.36	29.42	32.05	32.85
	20	27.98	28.60	28.05	28.19	28.11	29.10
Bridge	30	28.64	29.07	28.42	28.96	28.52	29.56
	40	28.94	29.25	28.60	29.32	28.68	29.74

Table 4

Image	SNR	$\epsilon = 0$		$\epsilon = \frac{1}{4}$	
		LSM	WAM	LSM	WAM
Boat	20	26.38	28.32	25.75	29.18
	30	26.61	28.47	26.00	29.32
	40	26.69	28.52	26.09	29.37
Bridge	20	25.47	25.52	25.51	26.18
	30	25.68	25.64	25.80	26.32
	40	25.76	25.69	25.92	26.36

Table 5

Image	SNR	$\epsilon = 0$			$\epsilon = \frac{1}{4}$		
		LSM	WAD	WAM	LSM	WAD	WAM
Boat	20	25.01	27.40	27.19	24.91	27.28	27.38
	30	25.12	27.53	27.32	25.05	27.40	27.49
	40	25.16	27.57	27.36	25.10	27.44	27.54
Bridge	20	24.04	24.51	24.20	24.21	24.39	24.57
	30	24.16	24.57	24.27	24.38	24.46	24.65
	40	24.21	24.60	24.30	24.45	24.48	24.68

Table 6
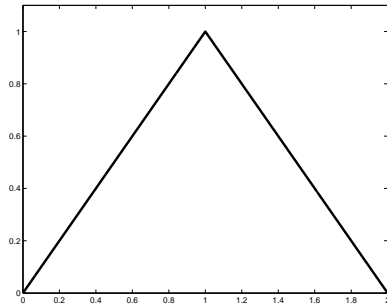
(a)
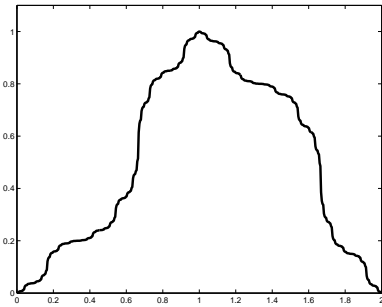
(b)
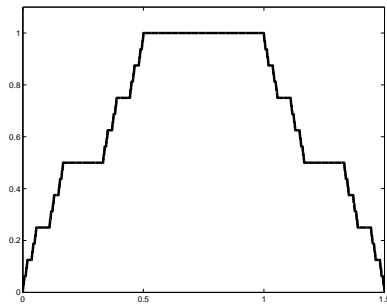
(c)
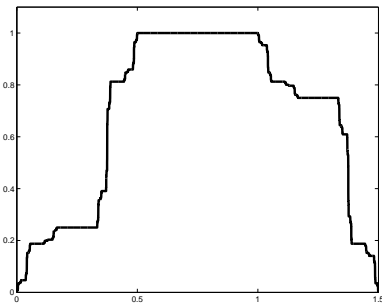
(d)
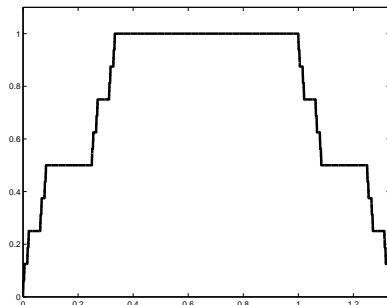
(e)
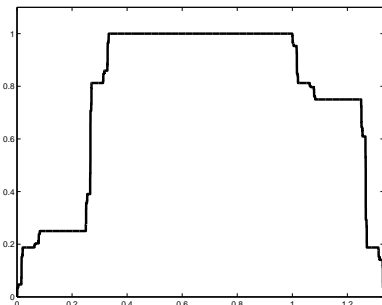
(f)
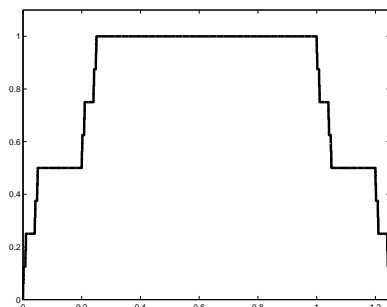
(g)
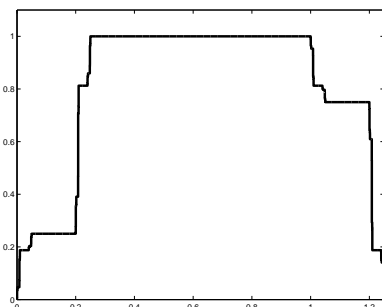
(h)

Figure 1
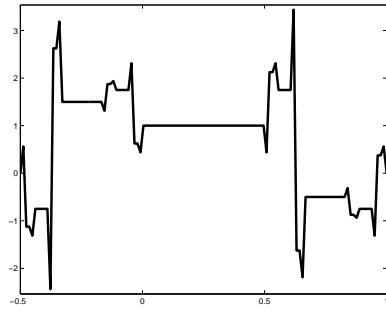
(a)
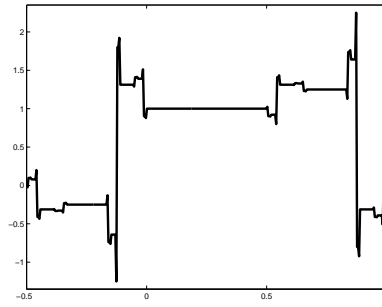
(b)
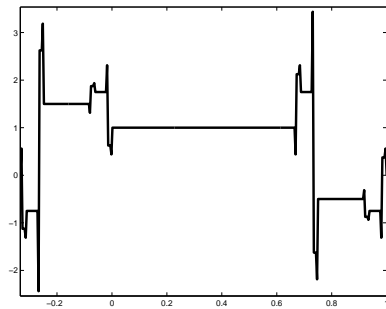
(c)
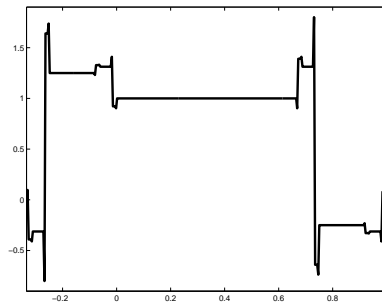
(d)
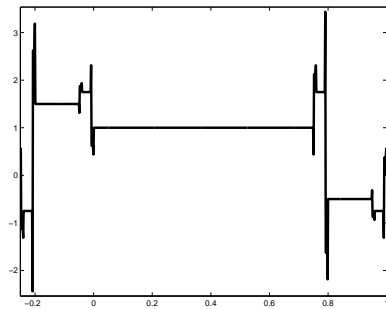
(e)
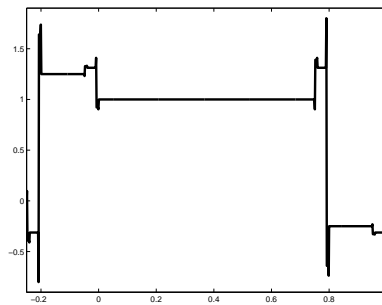
(f)

Figure 2

(a)   (b)

Figure 3

(a)

(b)

(c)

(d)

Figure 4

(a)

(b)

(c)

(d)

Figure 5

(a)

(b)

(c)

(d)

(e)

(f)

Figure 6
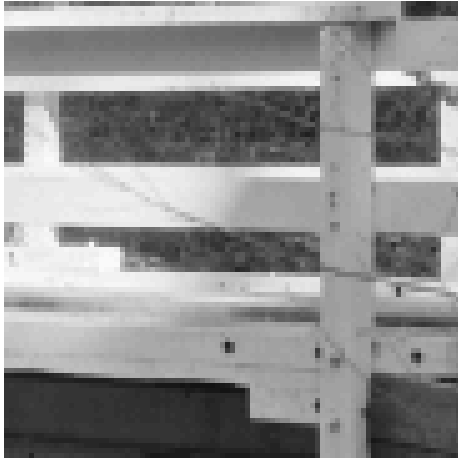
(a)
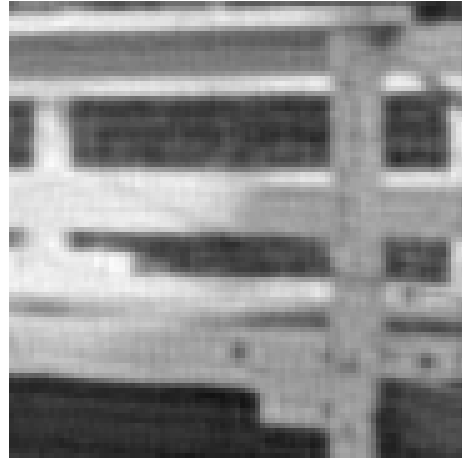
(b)
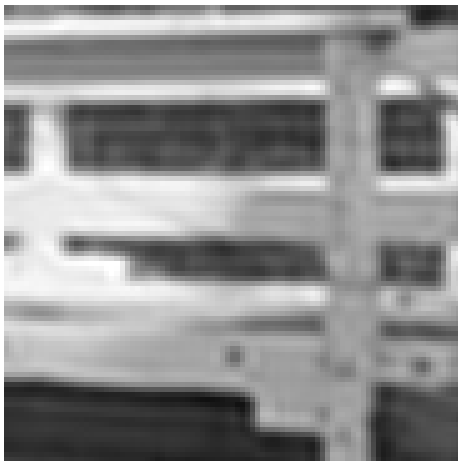
(c)
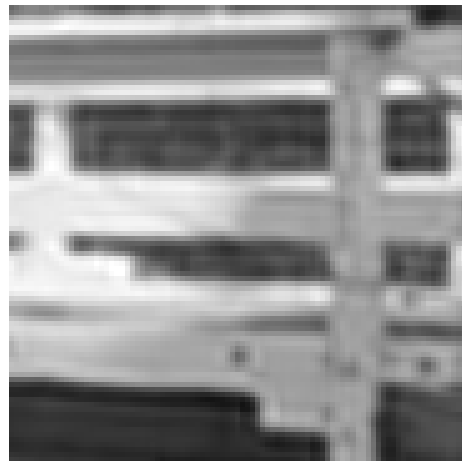
(d)

Figure 7

(a)　　　　　　　　　　　　　(b)

(c)　　　　　　　　　　　　　(d)

(e)　　　　　　　　　　　　　(f)

Figure 8